Supporting Information

An Efficient and Stable Deep-Blue Oxygen-Bridged Triphenylborane-Based Fluorophore with Hybridized Local and Charge-Transfer State

Jichen Lv,[a+] Jie Li,[a+] Shengnan Wang,[a] Haoran Shen,[a] Lifen Xia,[b] Yuchao Liu,[a] Shanfeng Xue,[a] Dongge Ma,[b] Shian Ying,[a*] and Shouke Yan[a, c*]

[a] Key Laboratory of Rubber-Plastics, Ministry of Education, Qingdao University of Science and Technology, Qingdao 266042, P. R. China.

[b] State Key Laboratory of Luminescent Materials and Devices, Guangdong Provincial Key Laboratory of Luminescence from Molecular Aggregates, Center for Aggregation-Induced Emission, South China University of Technology, Guangzhou 510640, P. R. China.

[c] State Key Laboratory of Chemical Resource Engineering, College of Materials Science and Engineering, Beijing University of Chemical Technology, Beijing 100029, P. R. China.

[+]J. Lv and J. Li contributed equally.

*Corresponding author: shian0610@126.com (S. Ying); skyan@mail.buct.edu.cn (S. Yan)

Experimental Section

1. General information

The initial raw materials and reagents were purchased without further purification in using process.

^{1}H and ^{13}C nuclear magnetic resonance (NMR) spectra were measured on a Bruker AVAN CE NEO 400 spectrometer by using tetramethyl silane (TMS) as the internal standard in chloroform-*d* ($CDCl_3$). High-resolution mass spectrum of molecule was measured by using a high-resolution quadrupole time of flight tandem mass spectrometer (TOF-MS). The atomic force microscopy (AFM) images were acquired by using a Bruker Dimension Icon. Ultraviolet-visible (UV-vis) absorption spectra in dilute solutions and neat films were measured by a HITACHI U-2910 spectrophotometer. The photoluminescence (PL) spectra in dilute solutions and films were recorded on a HITACHI F-4700 fluorescence spectrofluorometer. Transient lifetimes in dilute solutions and films were measured in a FLS1000 transient fluorescence spectrometer. Photoluminescence quantum yields (PLQYs) in dilute solutions and film were measured by the integration sphere setup (Hamamatsu C11347-11) equipped with a xenon high-pressure lamp. Differential scanning calorimetry (DSC) curves was obtained on a Netzsch DSC (204F1) instrument at a heating rate of 10 $^{o}C\ min^{-1}$ for two circulations. Cyclic voltammetry (CV) measured in dry dichlormethane (DCM) solution at room temperature was recorded at the scan rate of 100 $mV \cdot s^{-1}$ on a CHI660E electrochemical workstation with a conventional three-electrode system including a glass carbon working electrode, a platinum wire auxiliary electrode, and an Ag/Ag^{+} standard reference electrode. Tetrabutylammonium hexafluorophosphate (Bu_4NPF_6, 0.1 M) was acted as the supporting electrolyte and ferrocene served as the standard reference. The highest occupied molecular orbital (HOMO) energy level (E_{HOMO}) and the lowest unoccupied molecular orbital (LUMO) energy level (E_{LUMO}) can be calculated by the following formula:

$$E_{HOMO} = -(E_{ox} - E_{1/2}^{+} + 4.80)\ eV$$

$$E_{LUMO} = (E_{HOMO} + E_g)\ eV$$

Here, E_{ox} is the oxidation onset potentials relative to Ag/Ag^{+} electrode. $E_{1/2}^{+}$ is half wave potentials of Fc/Fc^{+} vs Ag/Ag^{+} acquired from the CV curves of oxidation and reduction. E_g is the optical bandgap evaluated from the onset of absorption spectrum.

2. Theoretical calculation

The optimized ground-state geometry, HOMO/LUMO distributions and energy levels were carried out by density functional theory (DFT) at the B3LYP/6-31G (d, p) level using Gaussian 16 package. At the same time,

singlet and triplet energy levels and natural transition orbitals (NTOs) were carried out by time-dependent DFT (TD-DFT) calculations at the B3LYP/6-31G (d, p) level using Gaussian 16 package. Multiwfn 3.8 was utilized to analyze the NTOs.[1] The spin-orbit coupling (SOC) matrix elements were calculated by TD-DFT at the B3LYP/6-31G (d, p) level using ORCA software package (Version 4.1).

3. OLED fabrication and measurement

Indium tin oxide (ITO) glasses with a sheet resistance of 15-20 Ω square^{-1} were ultrasonically treated in cleaner and deionized water, then dried for 30 mins at 120 °C in oven. After treated by oxygen plasma for 7 mins in a cleaning room, ITO substrates were put into the vacuum deposition system. Under the pressure of 2 × 10^{-4} Pa, the devices were fabricated with the evaporation rates of organic materials, lithium fluoride (LiF) and aluminum (Al) were 1-1.5, 0.2 and 5-10 Å s^{-1} via a shadow mask, detecting via a frequency counter and calibrated by a Dektak 6 M profiler (Veeco). The effective emission area of device was 3 mm × 3 mm. The current density-luminance-voltage curves were tested by the computer which controlled Keithley 2450 Series Digital Source-meter and LS160 Luminancemeter (KONICAMINOLTA). Electroluminescence (EL) spectra were measured by the optical analyzer FlAME-S-VIS-NIR photometer. And the external quantum efficiencies (EQEs) were calculated from the EL spectra, luminance, and current density.

4. Synthesis and characterizations

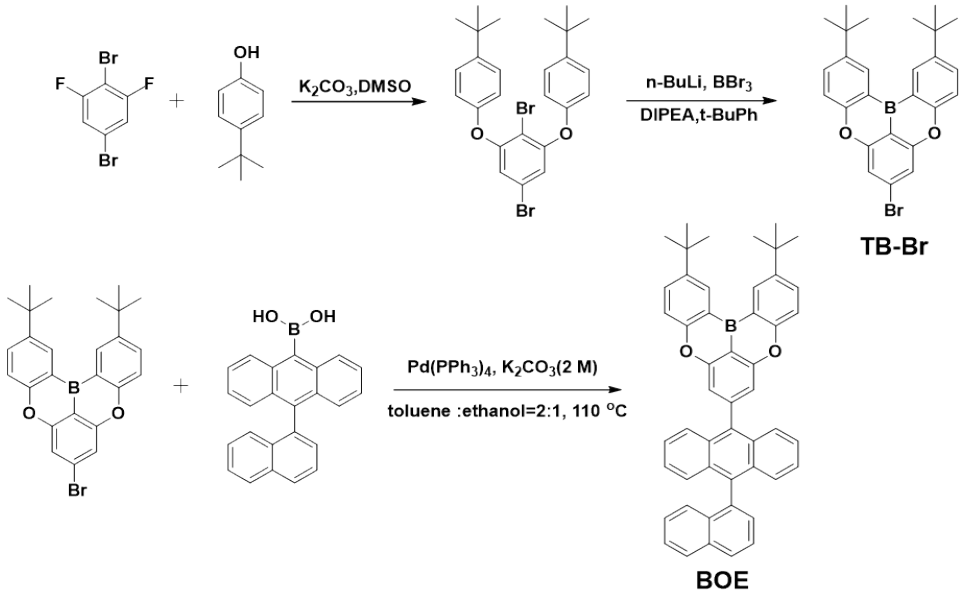

Scheme S1. Synthetic route and chemical structure of **BOE**.

Synthesis of 2,12-di-tert-butyl-7-(10-(naphthalen-1-yl) anthracen-9-yl)-5,9-dioxa-13b-boranaphtho[3,2,1-de]anthracene (BOE).

7-bromo-2,12-di-tert-butyl-5,9-dioxa-13b-boranaphtho[3,2,1-de]anthracene (TB-Br) was obtained following the procedures reported in our previous work.[2] TB-Br (1500 mg, 3.26 mmol), (10-(naphthalen-1-yl)anthracen-9-yl)boronic acid (1245 mg, 3.59 mmol), and tetrakis(triphenylphosphine)palladium (151 mg, 0.130 mmol) were put into a 250 mL two-necked flask. Under nitrogen atmosphere, toluene (20 mL), CH_3CH_2OH (10 mL) and 2M potassium carbonate solution (10 mL) were added. After stirred at 110 °C for 18 hours, the reaction mixture was cooled down to room temperature and extracted with CH_2Cl_2 and water. The organic layer was evaporated using a rotary evaporator under reduced pressure. The crude product was further purified by silica gel column chromatography using pure petroleum ether (PE) as eluent and recrystallization in chloroform. Finally, it was dried under vacuum to give a white solid (1518 mg, yield: 68%). ^{1}H NMR (400 MHz, $CDCl_3$) δ (ppm): 8.85 (d, *J* = 2.5 Hz, 2H), 8.09 (d, *J* = 8.2 Hz, 1H), 8.03 (d, *J* = 8.2 Hz, 1H), 7.82 (dd, *J* = 8.8, 1.8 Hz, 4H), 7.73 (dd, *J* = 8.2, 6.9 Hz, 1H), 7.62 (dd, *J* = 7.0, 1.3 Hz, 1H), 7.57 – 7.45 (m, 6H), 7.41 (d, *J* = 1.1 Hz, 1H), 7.33 (ddd, *J* = 8.8, 6.4, 1.3 Hz, 2H), 7.28 (dd, *J* = 8.5, 1.3 Hz, 1H), 7.25 – 7.18 (m, 3H), 1.53 (s, 18H). ^{13}C NMR (400 MHz, $CDCl_3$) δ (ppm): 158.85, 157.58, 157.57, 146.13, 145.15, 136.73, 136.62, 135.55, 133.74, 133.63, 131.60, 130.62, 130.35, 129.63, 129.27, 128.27, 128.19, 127.09, 126.97, 126.70, 126.37, 126.06, 125.63, 125.41, 125.30, 121.91, 118.14, 118.12, 111.66, 111.62, 34.63, 31.62. TOF-MS(ESI) m/z calcd. for C50H41BO2: 684.3200; $[M + H]^+$ found: 685.4382.

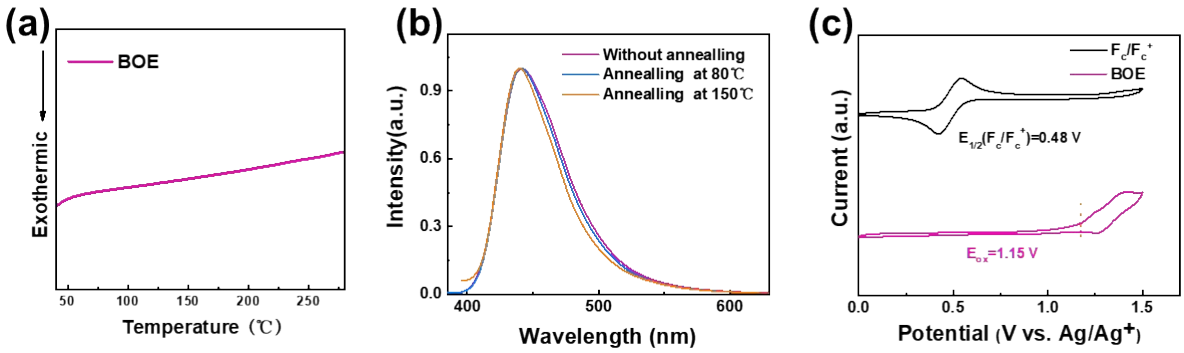

Fig. S1. (a) The DSC curve of **BOE**. (b) Normalized PL spectra of **BOE** at different annealed temperatures. (c) The CV measurement of **BOE**.

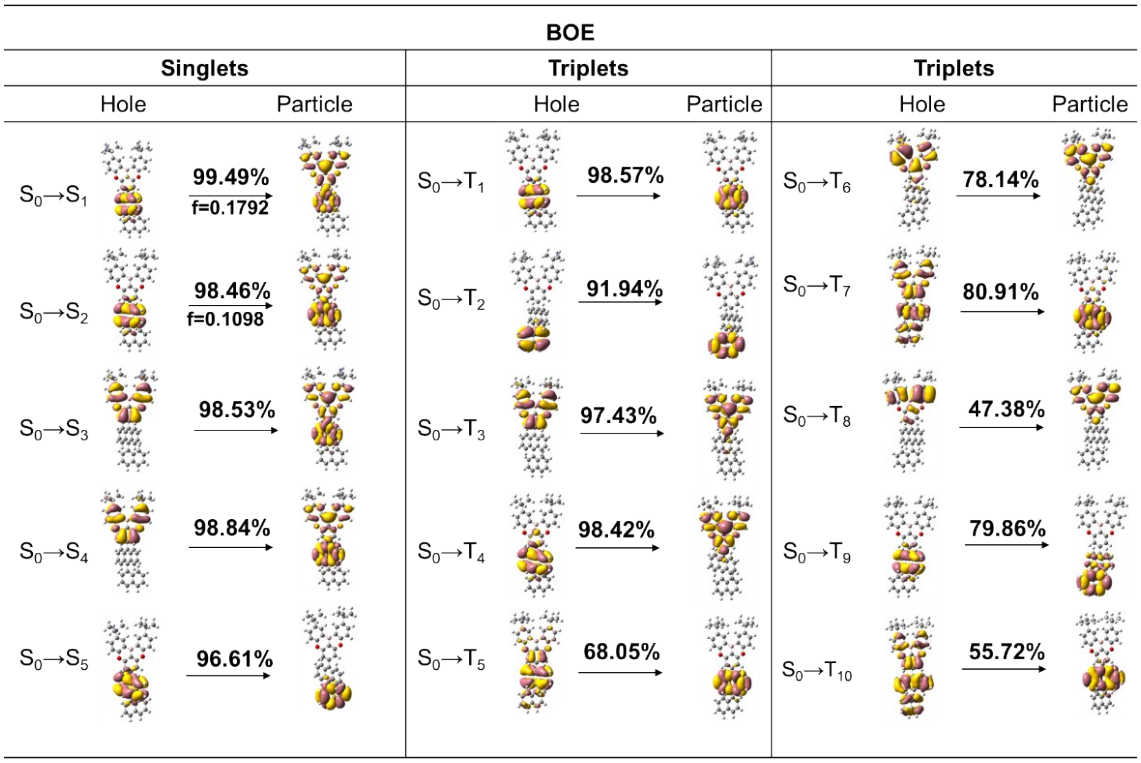

Fig. S2. The NTO distributions of singlet and triplet excited states for **BOE**.

Table S1. Computed singlet and triplet energy levels and oscillator strength of singlet states.

BOE				
Singlet states	**[eV]**	**Triplet states**	**[eV]**	**Oscillator strength of singlet states**
S_1	3.011	T_1	1.736	0.1792
S_2	3.196	T_2	2.705	0.1098
S_3	3.313	T_3	2.842	0.0783
S_4	3.460	T_4	3.040	0.0476
S_5	3.488	T_5	3.219	0.0000
S_6	3.497	T_6	3.319	0.0003
S_7	3.836	T_7	3.390	0.0001
S_8	3.913	T_8	3.437	0.0000
S_9	4.036	T_9	3.473	0.0196
S_{10}	4.219	T_{10}	3.493	0.0000

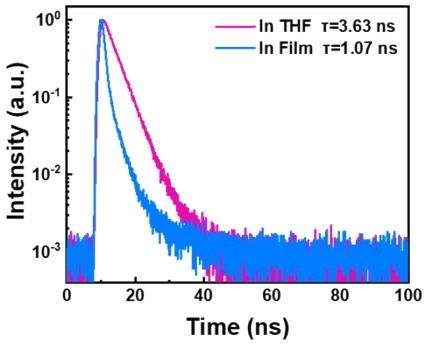

Fig. S3. Transient PL spectra of **BOE** in THF (10^{-5} M) and neat film.

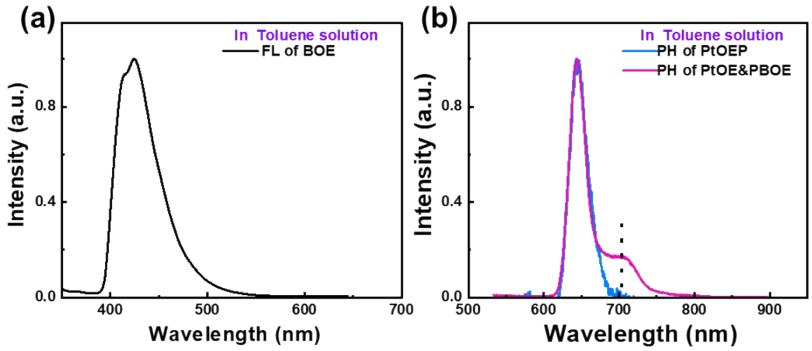

Fig. S4. (a) Low-temperature fluorescence in dilute THF solution (10^{-5} M) at 77 K. (b) Low-temperature phosphorescence spectra of platinum octaethylporphyrin (PtOEP, 10^{-5} M) and mixture solution of PtOEP (10^{-5} M) and **BOE** (10^{-3} M) at 77 K.

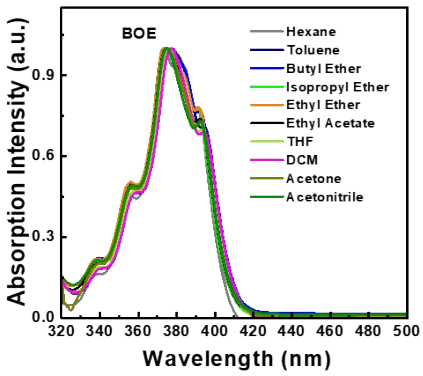

Fig. S5. The normalized UV–vis spectra of **BOE** in different solvents (10^{-5} M).

Table S2. The absorption and emission data of BOE in different polar solvents.

Solvents	ε	n	f(ε, n)	λ_a (nm)	λ_f (nm)	ν_a- ν_f (cm^{-1})
Hexane	1.9	1.375	0.0012	373	420.4	3022.782
Toluene	2.38	1.494	0.013	378	428.8	3134.131
Triethylamine	2.42	1.401	0.048	375	423.8	3070.631
Butyl ether	3.08	1.399	0.096	376	426.2	3132.582
Isopropyl ether	3.88	1.368	0.145	374	424.8	3197.478
Ethyl ether	4.34	1.352	0.167	374	425.2	3219.624
Ethyl acetate	6.02	1.372	0.2	375	430.2	3421.664
Tetrahydrofuran	7.58	1.407	0.21	376	432	3447.597
Dichloromethane	8.93	1.424	0.217	377	435.2	3547.258
Acetone	20.7	1.359	0.284	375	439	2499.359
Acetonitrile	37.5	1.344	0.305	375	443.8	3887.623

Detailed Lippert-Mataga Calculation

The Stokes shift ($\nu_A - \nu_f$) versus orientational polarizability ($f(\varepsilon, n)$) of solvents can be constructed by the Lippert-Mataga model with the Equation 1 as below.

$$hc(\nu_A - \nu_f) = hc(\nu_A^0 - \nu_f^0) + \frac{2(\mu_e - \mu_g)^2}{a_0^3} f(\varepsilon,n) \quad (1)$$

Here, h is the Plank constant, c is the light speed in vacuum, μ_g and μ_e are the ground-state excited-state dipole moments, $f(\varepsilon, n)$ is the orientational polarizability of solvents, a_0 is the Onsager cavity radius, $\nu_A^0 - \nu_f^0$ is the Stokes shifts when f is zero, respectively.

Take differential on both sides of the Equation 1, the Equation 2 can be obtained:

$$\mu_e = \mu_g + \{\frac{hca_0^3}{2} \times [\frac{d(\nu_A - \nu_f)}{df(\varepsilon, n)}]\}^{1/2} \quad (2)$$

f(ε, n) and a_0 can be obtained by the Equation 3 and 4:

$$f(\varepsilon,n) = \frac{\varepsilon - 1}{2\varepsilon + 1} + \frac{n^2 - 1}{2n^2 + 1} \quad (3)$$

$$a_0 = (\frac{3M}{4\pi Nd})^{1/3} \quad (4)$$

Where, ε and n are dielectric constant and refractive index of solvent, N is Avogadro's number, M is molar mass, and d is density of the solvents, respectively. The values of f(ε, n) and a_0 can be estimated by the Equation 3 and 4. The μ_g of BOE (1.440 Debye) was estimated with the Gaussian 16 package at the level of B3LYP/6-31G(d, p). The $\frac{d(\nu_A - \nu_f)}{df(\varepsilon, n)}$ can be estimated with the solvatochromic experiment data listed in Table S2. With the information above, the Stokes shift versus orientation polarizability curves of both two compounds show two-section linear relations in low- and high-polar solvents (Figure 3c), belonging to the typical HLCT excited state characteristic, which is beneficial to improve the exciton utilization efficiency in the electroluminescence process.

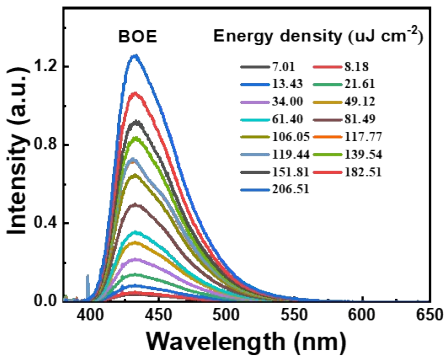

Fig. S6. Dependence of PL spectra on the different excitation laser fluence of **BOE**.

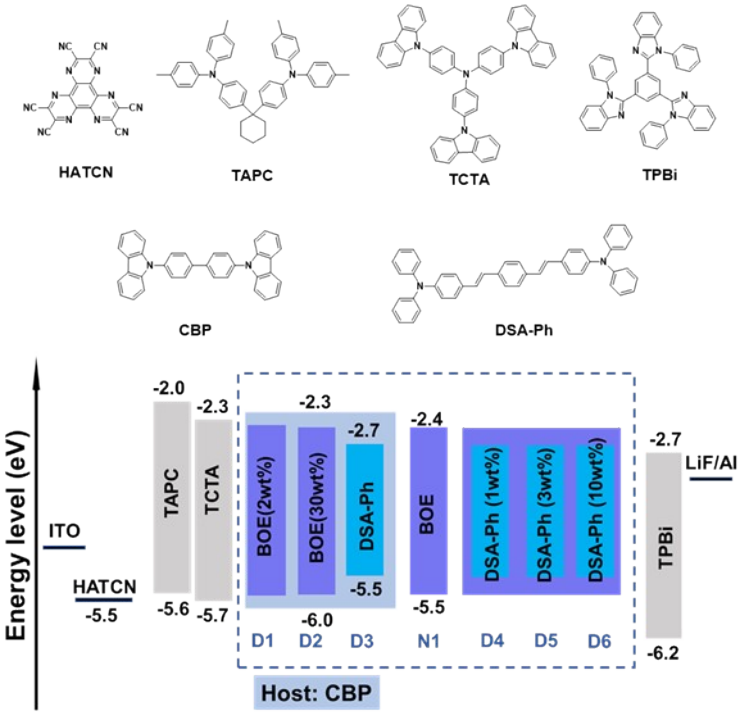

Fig. S7. Chemical structures and energy diagrams of materials used in this work.

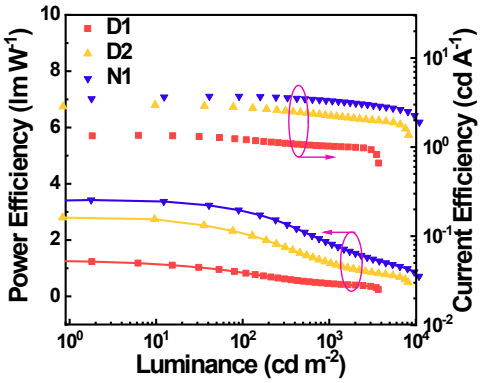

Fig. S8. Power efficiency-luminance-current efficiency curves for devices **D1**, **D2** and **N1**.

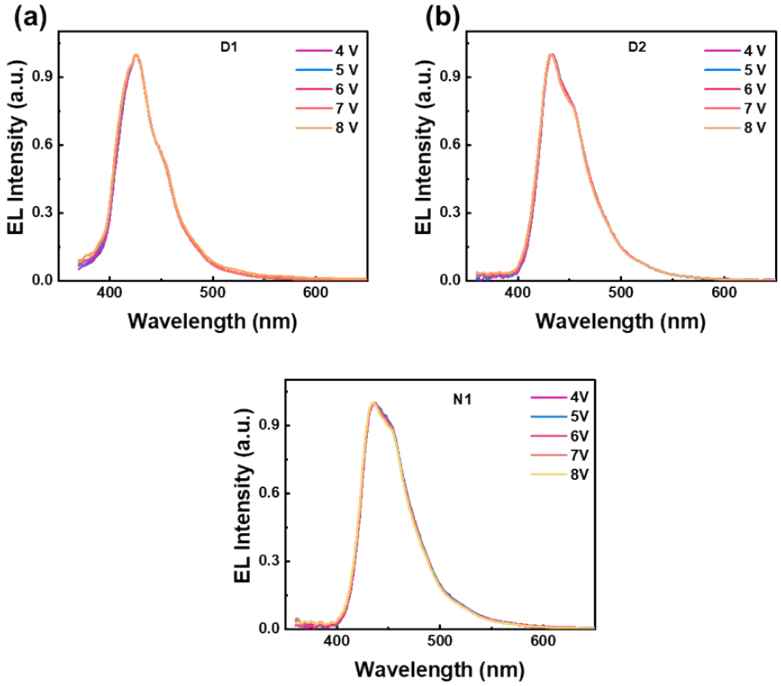

Fig. S9. EL spectra of devices D1 (a), D2 (b), and N1 (c).

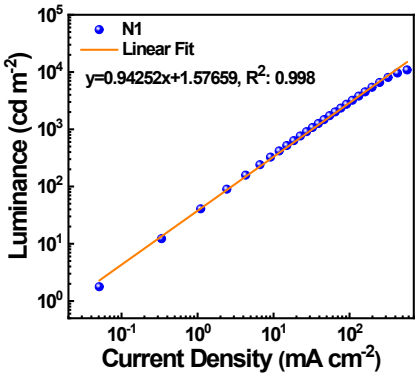

Fig. S10. Luminance-current density curve and its linear fit for device **N1**.

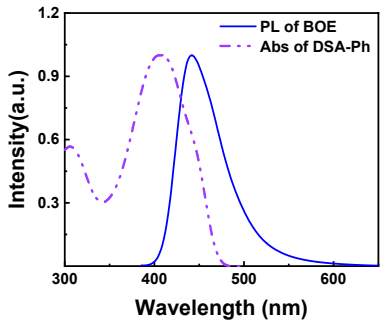

Fig. S11. Absorption spectrum of DSA-Ph film and PL spectrum of **BOE** film.

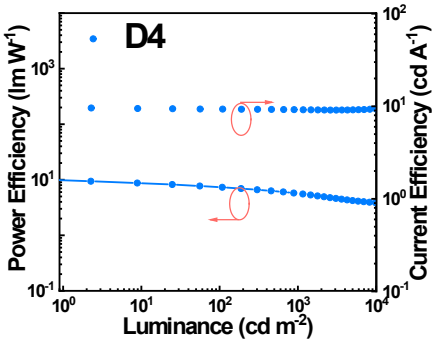

Fig. S12. Power efficiency−luminance−current efficiency curves of device **D4**.

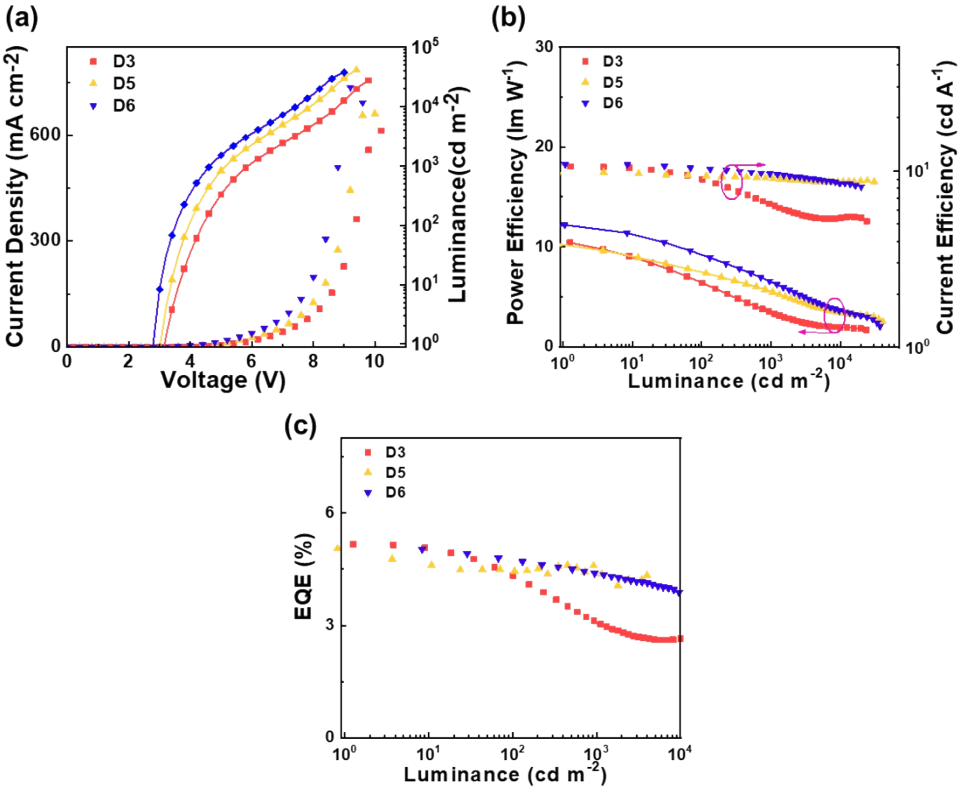

Fig. S13. (a) Current density–voltage–luminance curves of devices **D3**, **D5**, and **D6**. (b) Power efficiency−luminance−current efficiency curves of devices **D3**, **D5**, and **D6**. (c) EQE versus luminance curves of devices **D3**, **D5**, and **D6**.

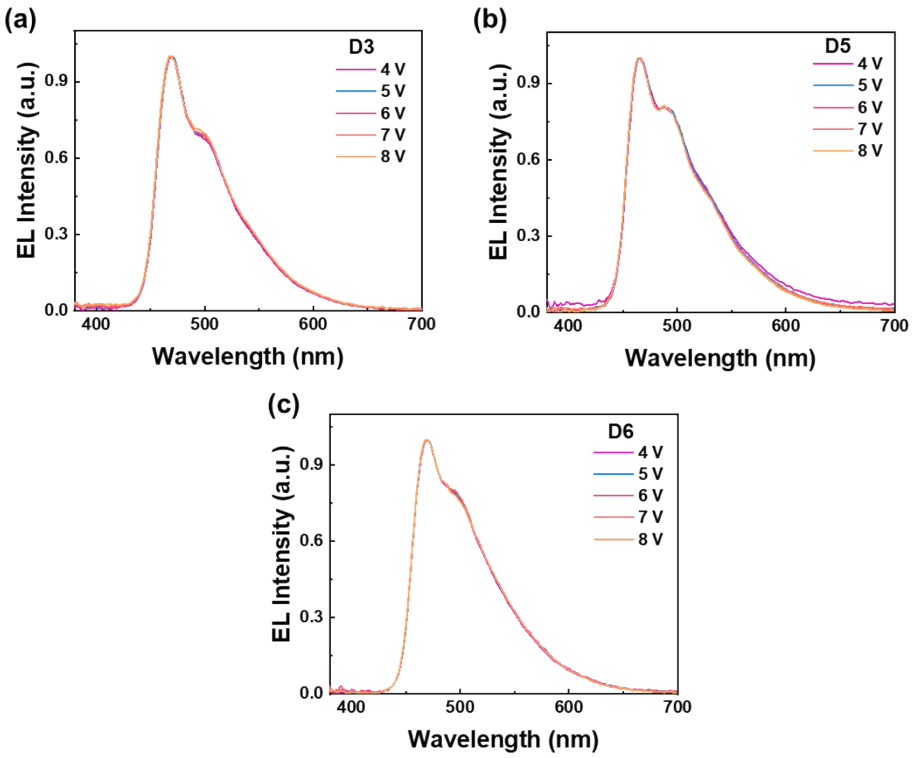

Fig. S14. EL spectra of devices **D3** (a), **D5** (b), and **D6** (c).

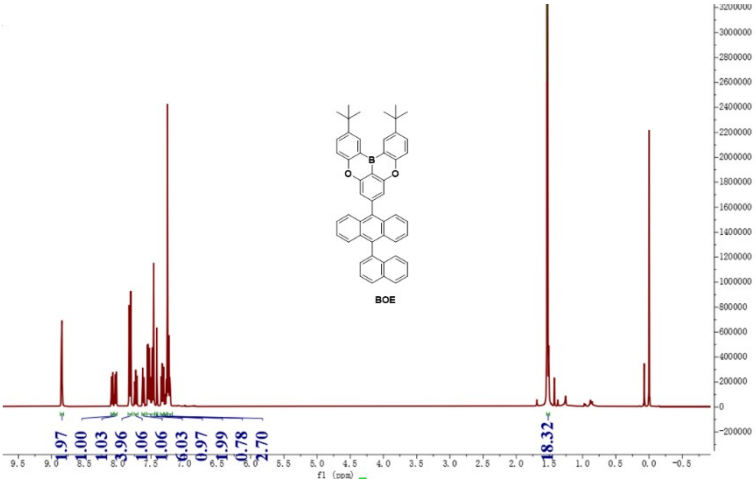

Fig. S15. ^{1}H NMR spectrum of the target compound BOE.

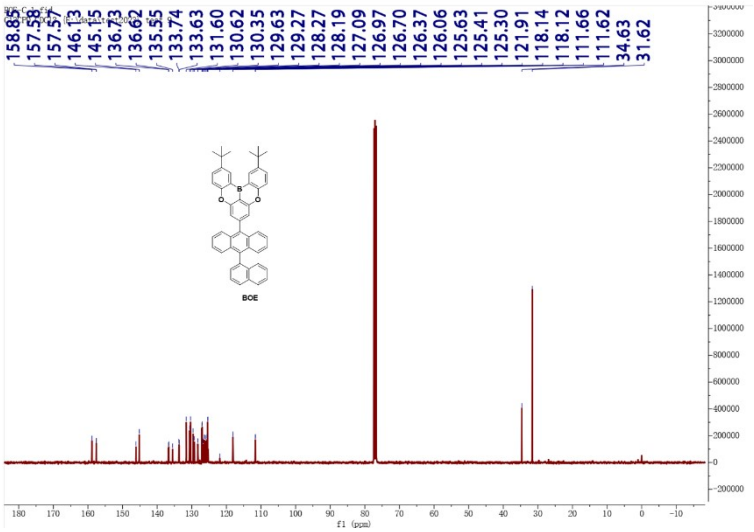

Fig. S16. ^{13}C NMR spectrum of the target compound BOE.

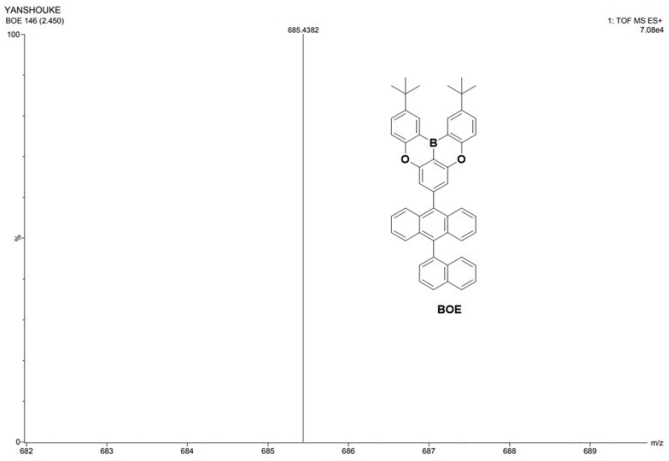

Fig. S17. TOF-MS spectrum of the target compound BOE.

Notes and references

1 T. Lu and F. Chen, Multiwfn: A multifunctional wavefunction analyzer, *J. Comput. Chem.*, 2012, **33**, 580-592.

2. Y. Xie, L. Hua, Z. Wang, Y. Liu, S. Ying, Y. Liu, Z. Ren and S. Yan, Constructing an efficient deep-blue TADF emitter by host-guest interactions towards solution-processed OLEDs with narrowband emission, *Sci. China: Chem.*, 2023, **66**, 826-836.